Epoxy-Layered Silicate Nanocomposites and Their Gas Permeation Properties

Maged A. Osman,[†] Vikas Mittal,[†] Massimo Morbidelli,[‡] and Ulrich W. Suter*[,†]

Department of Materials, Institute of Polymers, and Department of Chemistry and Applied Biosciences, Institute of Chemical and Bioengineering, ETH Zurich, CH-8093 Zurich, Switzerland

Received June 17, 2004

ABSTRACT: Epoxy-OM (organo-montmorillonite) nanocomposites have been synthesized, and their permeability to oxygen and water vapor has been measured. The chemical structure of the organic monolayer ionically bonded to the montmorillonite surface has been varied, and its influence on the swelling, intercalation, and exfoliation behavior of the OM has been studied. Exfoliated aluminosilicate layers build a barrier for the permeating gas molecules, while the polymer intercalated tactoids do not contribute much to the permeation barrier performance. The gas permeation through the composites was correlated to the volume fraction of the impermeable inorganic part of the OM. The incorporation of small volume fractions of the platelike nanoparticles in the polymer matrix decreased its permeability coefficient when the interface between the two heterogeneous phases was properly designed. Long alkyl chains enhanced the polymer intercalation but increased the permeability coefficient probably due to phase separation at the interface between the polymer and the inclusions. Matching the surface energy of the OM with that of the matrix as well as tethering polymer molecules to the silicate layers surface enhanced the exfoliation and decreased the permeation coefficient. The exfoliation process is governed by interplay of entropic and energetic factors. A macroscopic volume average of the aspect ratio of montmorillonite platelets was deduced from the relative permeability of the nanocomposites by comparing the measured values to numerical predictions of gas permeation through composites of misaligned disk-shaped inclusions. The permeability coefficient of the epoxy matrix was reduced to one-fourth at 5 vol % Bz1OH loading, and the reduction was attributed to the tortuous pathway the gas molecules have to cover during their random walk to penetrate the composite. The transmission rate of water vapor through the composites is more influenced by the permeant−composite interactions and hence the hydrophobicity of the monolayer covering the inclusions surface. At 5 vol % BzC16 loading, the relative vapor transmission rate was reduced to half.

Introduction

Polymer nanocomposites are nanoscale materials, in which at least one of the components has a dimension smaller than 100 nm. They offer an opportunity to explore new behaviors and functionalities beyond that of conventional materials. The inclusion of nanoparticles with huge surface area and often anisotropic geometry in a polymer matrix leads to increased particle−matrix interactions and decreased interparticle distances with consequent changes in morphology and performance.[1] Significant improvements in permeability, thermal stability, flame retardency, and mechanical and dielectric properties have been observed at low filler volume fraction.[2−7] An important attribute of nanocomposites is that performance enhancement is achieved without impairing the optical homogeneity and density of the material. Aluminosilicates and especially montmorillonite, which can be exfoliated to 1 nm thick platelets, have been frequently used to prepare polymer nanocomposites. To render the hydrophilic surface of montmorillonite compatible with polymers, its inorganic cations are usually exchanged with organic ammonium ions to give organo-montmorillonite (OM).[8,9]

Polymers are currently used in packaging applications, especially in food and drug packaging, where transparency and gas-barrier properties are important criteria. Often laminates of a polyolefin, serving as humidity barrier, and PET, serving as oxygen barrier, are used. The two foils are usually held together by an adhesive, which does not contribute much to the barrier performance of the laminate. Epoxy resins are thermoset polymeric materials, which received special attention as adhesives.[10,11] Several efforts have been made to enhance their permeation barrier properties through molecular design.[12,13] Another promising approach to improve their barrier properties has become feasible by the progress in nanocomposites. By incorporating impermeable transparent platelike nanoparticles in the polymer matrix, the permeating molecules are forced to wiggle around them in a random walk, hence diffusing through a tortuous pathway.[14−16] The decrease in transmission rate of the permeant is a function of the aspect ratio of the inclusions, their volume fraction, and orientation. The synthesis of epoxy−clay nancomposites has been extensively studied, and enhanced mechanical properties were reported.[17−24] However, the permeation properties of epoxy nanocomposites have not yet been reported. Exfoliated and intercalated morphologies have been observed and associated with the curing rate inside and outside the interlayer of the OM, which is often carried out at high temperatures. The absence of reflections below 7° 2Θ in the wide-angle X-ray diffraction (WAXRD) is usually considered as an evidence of exfoliation although this is not necessarily true.[7,25,26] The improvement in mechanical properties was ascribed to the high aspect ratio of exfoliated silicate layers.

[†] Department of Materials, Institute of Polymers.
[‡] Department of Chemistry and Applied Biosciences, Institute of Chemical and Bioengineering.
* Corresponding author: Ph +41 1 632 2039; Fax +41 1 632 1592; e-mail uwsuter@eth.ch.

10.1021/ma048798k CCC: $27.50
Published on Web 08/21/2004

The objective of the present investigation is to prepare epoxy-OM nanocomposites and to study their oxygen and water vapor permeation properties with the perspective of using them in laminate production or in coating polyolefin foils to improve their oxygen-barrier performance. The epoxy resin and the curing agent were chosen to provide a polymer matrix that meets the requirements of the food-and-health regulations and has low gas permeability. The curing temperature has also to be kept low in order not to deform the substrate foils. Since the inorganic part of the OM is that which is impermeable, the reduction in permeability is correlated with its volume fraction. The relative oxygen permeability is compared to numerical predictions, and a macroscopic average aspect ratio of the inclusions is deduced thereof. The study also includes an investigation of the influence of the chemical structure of the organic monolayer ionically bonded to the clay surface as well as that of filler loading on the barrier properties of these nanocomposites.

Experimental Section

Materials. Purified sodium bentonite (Cloisite Na^+) was purchased from Southern Clay Products (Gonzales, TX). The epoxy resin, bisphenol A diglycidyl ether (4,4′-isopropylidenediphenol diglycidyl ether) with an epoxide equivalent weight 172−176, was supplied by Sigma (Buchs, Switzerland). Dioctadecyldimethylammonium chloride (2C18), triethanolamine, *N*-butyldiethanolamine, 2-(dibutylamino)ethanol, 1-bromooctadecane, benzyl chloride, tetraethylenepentamine (TEPA), tetrahydrofuran (THF), and dimethylformamide (DMF) were procured from Fluka (Buchs, Switzerland). *N*-Benzyl-*N*-methylethanolamine was supplied by Aldrich (Buchs, Switzerland), while benzyldimethylhexadecylammonium chloride (BzC16) was purchased from Acros Organics (Basel, Switzerland). Polypropylene (100 μm thick) and polyamide (15 μm thick) foils, whose surface was corona-treated to enhance their wetting and adhesion, were kindly supplied by Alcan Packaging (Neuhausen, Switzerland). A surfactant (trade name BYK-307) was used to achieve better wetting and adherence of the neat epoxy coating to the substrate foils and was obtained from Christ Chemie (Reinach, Switzerland).

Synthesis of the Ammonium Salts. Some of the ammonium salts used to modify the montmorillonite surface are not commercially available. Benzyldibutyl(2-hydroxyethyl)-ammonium chloride (Bz1OH), benzylbis(2-hydroxyethyl)butylammonium chloride (Bz2OH), benzyltriethanolammonium chloride (Bz3OH), and benzyl(2-hydroxyethyl)methyloctadecylammonium chloride (BzC18OH) were synthesized by quaternizing the corresponding amines with alkyl halides (benzyl chloride and 1-bromooctadecane).[27−31] Generally, the alkyl halide (0.105 mol) was slowly added to an alcoholic solution of the amine (0.1 mol in 50 mL), and the mixture was stirred overnight under reflux. The product was purified by extracting it twice with ether after evaporating the ethanol. The obtained quaternary ammonium salts were recrystallized from acetone: Bz1OH, mp 137 °C; Bz2OH, mp 105 °C; Bz3OH, mp 80 °C; BzC18OH, mp 110 °C.

Surface Treatment of Montmorillonite. The cation exchange capacity (CEC) of Cloisite Na^+ was determined by exchanging its sodium ions with $Cu(trien)^{2+}$ to be 0.88 mequiv/g.[32,33] The aluminosilicate surface was rendered organophilic by exchanging its inorganic cations with organic ammonium ions, viz., Bz1OH, Bz2OH, Bz3OH, BzC18OH, 2C18, and BzC16. An 8 g sample of Cloisite Na^+ was stirred in 500 mL of deionized water at 70 °C for 2 h, and then 200 mL of ethanol was added. The aluminosilicate was dispersed by sonication for 10 min (ultrasonic horn at 70% amplitude) followed by shear mixing for 10 min (Ultra-Turax T50, IKA, Staufen, Germany). To this dispersion, a solution of the desired ammonium salt corresponding to 150% of the clay's CEC in 100 mL of ethanol was added dropwise (within 2 h) under stirring. The reaction mixture was stirred overnight at 70 °C, and the product was filtered and washed halogen free with a hot water−ethanol mixture (1:1) and then hot ethanol. To remove all nonreacted or intercalated (local bilayer) molecules, the product was suspended in a solvent, in which optimal swelling of the OM is achieved. The suspension was sonicated for 5 min and stirred overnight at 70 °C, then filtered, washed, and dried at 70 °C under reduced pressure. The degree of exchange and the purity of the product were monitored by Hi-Res TGA.[9,33] If the mass loss in the TGA did not correspond to full ion exchange, the exchange reaction was repeated. The OM was finally suspended in 500 mL of dioxane, sonicated, and freeze-dried. In the following, the modified clay is given the acronym of the organic cation attached to its surface.

Thermogravimetric Analysis. High-resolution (Hi-Res) thermogravimetric analysis (TGA) of the modified fillers, in which the heating rate is coupled to the mass loss, that is, the sample temperature is not raised until the mass loss at a particular temperature is completed, was performed on a Q500 thermogravimetric analyzer (TA Instruments, New Castle, DE). All measurements were carried out under an air stream in the temperature range 50−900 °C. Quantitative analysis of the organic monolayer on the montmorillonite surface was achieved by subtracting the mass loss due to physisorbed water and to dehydroxylation of the mineral from the total mass loss.[9]

Nanocomposite Preparation. The required amounts of OM and epoxy resin were calculated on the basis of the desired inorganic volume fraction as follows:

$$M_{OM} = M_M + (M_M \mathrm{CEC} M_{OC})$$

$$M_{EP} = \frac{M_M V_{EP} \rho_{EP}}{V_M \rho_M} - (M_M \mathrm{CEC} M_{OC})$$

where M_{OM} is the mass of the OM, M_M is the mass of the inorganic aluminosilicate, M_{OC} is the molar mass of the ammonium ion used to modify the montmorillonite surface, M_{EP} is the mass of the epoxy resin, V_M is the inorganic volume fraction, ρ_M is the density of sodium montmorillonite (2.6 g/cm^3), V_{EP} is the epoxy volume fraction, and ρ_{EP} is its density (1.18 g/cm^3).

The necessary amount of OM was added to 25 g of solvent (THF or DMF) and allowed to swell for 2 h. The suspension was cooled in an ice bath and sonicated (ultrasound horn) twice at 70% amplitude for 5 min each time with 5 min pause in between. The epoxy resin solution (5.3 g in 5 g of solvent) was mixed with the OM suspension, and the mixture was allowed to stand for 2 h, after which the sonication process was repeated. The curing agent, i.e., TEPA (0.9 g), was then added and thoroughly mixed with the epoxy−clay mixture. To achieve a slow curing rate, favorable for exfoliation, the amine to epoxy mole ratio was maintained at 0.3:1. The suspension was shortly sonicated to degas it, and a film was drawn on the corona-treated surface of PP and PA foils with the help of a bar coater (90 μm gap). The coated films were dried at ambient conditions for 15 min and under reduced pressure at RT for another 15 min, then cured at 70 °C overnight, and postcured at 90 °C for 4 h. A low curing temperature was chosen to achieve slow curing favorable for exfoliation. In the case of the neat epoxy, it was necessary to add 2 mg of a surfactant (BYK-307) to improve the quality of the coating. The thickness of the dry coated film was ca. 10 μm, and its correct thickness was determined as described below.

Density and Thickness. The density of the substrate foils (PP and PA) and the neat epoxy resin was determined by weighing samples in air and in ethanol using an analytical balance (Mettler AE 200) and a homemade device similar to the Mettler density kit ME-33360 following the equation

$$\rho = \frac{\rho_{Et} M}{M - M_l}$$

where ρ is the sample density, ρ_{Et} is the density of ethanol at

22 °C, M is the sample mass in air, and M_l is its mass in ethanol. The thickness of the substrate foils was calculated from the weight of a piece of defined area and its density. The average of five measurements was taken.

The thickness of the coated film (t_f) was similarly determined as follows:

$$t_f = (M_1 - M_2)/(\rho_c A)$$

where M_1 is the mass of the coated foil, M_2 is the mass of an uncoated foil with the same area, ρ_c is the density of the composite, and A is the area of the foil. The density of the composite was calculated as

$$\rho_c = \frac{1}{\frac{m_{OM}}{\rho_{OM}} + \frac{m_{EP}}{\rho_{EP}}}$$

where m_{OM} is the mass fraction of the OM, ρ_{OM} is its density, m_{EP} is the mass fraction of the cured epoxy resin, and ρ_{EP} is its density. The density of the OM was analogously calculated from that of the organic monolayer (assumed to be equivalent to that of octadecanol = 0.81 g/cm^3) and that of sodium montmorillonite. The organic and inorganic mass fractions in the OM were calculated from the CEC and the molar mass of the organic cation.

Gas Permeation. The oxygen transmission rate through PP foils coated with the neat epoxy and the nanocomposites was measured using an OX-TRAN 2/20 ML (Mocon, Minneapolis, MN) at 23 °C and 0% RH. The water vapor transmission rate through PA foils coated with neat epoxy or nanocomposites was measured using a PERMATRAN-W 3/31 MG (Mocon, Minneapolis, MN) at 23 °C and 100% RH. The PP and PA substrates were selected on the basis of their high transmission rate for the specific permeant so that they do not hinder measuring the permeation through the coated film. The total transmission rate (T_{tot}) of oxygen or water vapor was normalized with respect to the total thickness (t_{tot}), and the transmission rate through the neat epoxy or nanocomposite films was calculated as follows:

$$t_{tot}/T_{tot} = t_1/T_1 + t_2/T_2$$

where t_i are the thicknesses of the coated film and the substrate foil and T_i are the corresponding normalized transmission rates. The average of four measurements for each coating is reported.

Wide-Angle X-ray Diffraction (WAXRD). Wide-angle X-ray diffraction patterns were collected on a Scintag XDS 2000 diffractometer (Scintag Inc., Cupertino, CA) using Cu Kα radiation (λ = 0.154 06 nm) in reflection mode. The instrument was equipped with a graphite monochromator and an intrinsic germanium solid-state detector. The coated foils and the suspensions were step-scanned (step width 0.02° 2Θ, scanning rate 0.06°/min) at room temperature from 1.5° to 10° 2Θ. The OMs were step scanned at a higher rate (0.24°/min) in the range 1.5°−30° 2Θ. The (001) basal-plane reflection of an internal standard muscovite (very thin platelets, 2Θ = 8.84°) was used to calibrate the line position of the OM reflections. To determine the peak positions, the diffractograms were fitted with a split Pearson VII function (diffraction management system software 1.36b).

Transmission Electron Microscopy (TEM). The microstructure of the nanocomposites was studied by bright-field TEM using a Zeiss EM 912 Omega microscope. Pieces of the coated foils were etched with oxygen plasma for 3 min and embedded in an epoxy matrix (Epon 812 + Durcopan ACM 3:4, Fluka, Buchs, Switzerland). 50−100 nm thick sections were microtomed with a diamond knife (Reichert Jung Ultracut E). The sections were supported by 100 mesh grids sputter-coated with a 3 nm thick carbon layer.

Results and Discussion

To reduce the surface energy and hydrophilicity of the clay, hence rendering it compatible with the epoxy matrix, its inorganic cations were exchanged with organic ammonium ions of different chemical structures. Dioctadecylammonium (**I**), benzylhexadecylammonium (**II**), and benzylhydroxyethyloctadecylammonium (**III**) as well as mono- (**IV**), di- (**V**), and triethylhydroxyammonium (**VI**) moieties were chosen for this purpose (Figure 1). Long alkyl chains increase the *d*-spacing, thus facilitating the penetration of guest molecules in the interlayer and consequently the intercalation and exfoliation. The benzyl group is expected to lead to stronger van der Waals attraction forces between the filler and the epoxy resin that enhances the intercalation and exfoliation of the clay particles. The hydroxyethyl groups were chosen to match the polarity of the EP matrix and because it may react with the epoxy groups of the resin, thus tethering polymer chains to the silicate layers. Tethered polymer molecules expand the interlayer and cannot be squeezed out if the silicate layers collapse, hence enhancing intercalation or exfoliation of the OM. The formation of local bilayer during surface treatment of the clay was avoided because the presence of unreacted molecules intercalated in the organic monolayer of the OM in a tail-to-tail arrangement, i.e., with their polar headgroups pointing outward, is expected to influence the surface energy and reduce the thermal stability of the OM.[9] Because of the high CEC of montmorillonite and the large molecular weight of the organic cations, the density of the OM is significantly lower than that of sodium montmorillonite and should be taken into consideration on calculating the volume fraction. Table 1 gives the densities of the different OMs prepared and their weight fraction that correspond to 0.035 inorganic volume fraction as well as the densities of the nanocomposites.

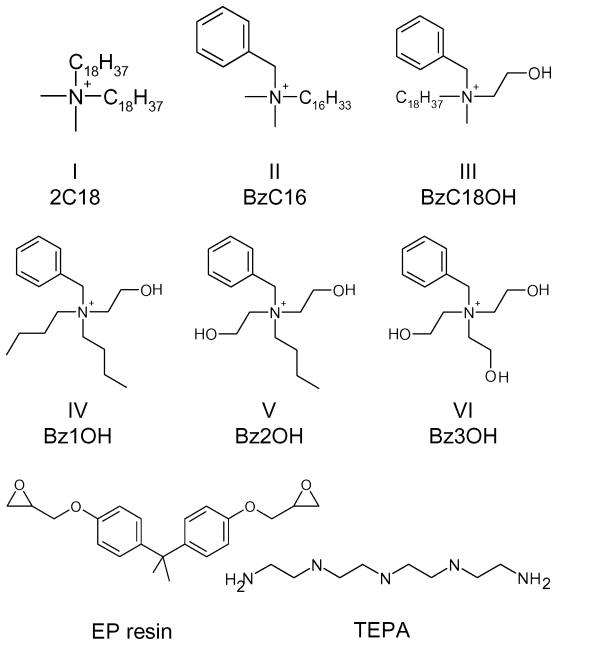

Figure 1. Chemical structure of the ammonium ions used to organophylize the montmorillonite surface as well as that of the epoxy resin and its curing agent.

Depending on the length of the alkyl chains, the cross-sectional area of the organic cations, and the available area per cation on the clay surface, the *d*-spacing of the layered silicate is expanded to different extents.[33] A large basal-plane spacing facilitates polymer intercalation and reduces the attraction forces between the silicate layers, leading to exfoliation of the OM. Table

Table 1. Density of the Organo-Montmorillonites and Their 3.5 vol % Composites

OM	modified filler density [g/cm^3]	filler weight fraction [%]	composite density [g/cm^3]
Bz1OH	1.93	8.96	1.22
Bz2OH	2.01	8.89	1.23
Bz3OH	2.13	8.82	1.23
BzC18OH	1.63	9.85	1.21
BzC16	1.69	9.51	1.21
2C18	1.53	10.60	1.21

2 shows that the *d*-spacing of the OM was modestly influenced by the short alkyl chains of Bz1OH, Bz2OH, and Bz3OH but was strongly expanded by the long alkyl chains of BzC16, BzC18OH, and 2C18. The preparation of the composites included swelling of the OM in an organic solvent and sonication to disintegrate the clay particles into its primary layers. X-ray measurements of these suspensions (Table 2) showed that all clays including the sodium montmorillonite swelled in DMF to different extents, leading to an increase in *d*-spacing, whereby the ones carrying long alkyl chains swelled more. Only the diffractogram of the BzC16 suspension was "silent", indicating that the clay was exfoliated to such an extent that no thick enough stacks (tactoids) in detectable concentration were present. The degree of swelling seems to depend on the clay solvatization, i.e., on the solubility parameters of the monolayer and the solvent.[34,35] Addition of the epoxy resin to the OM suspension did not affect the *d*-spacing of Bz1OH and Bz2OH but decreased that of Bz3OH by 0.16 nm, indicating a better match between the epoxy resin and Bz1OH or Bz2OH. The *d*-spacing of BzC18OH and 2C18 was decreased by 0.23 and 0.15 nm, respectively, on adding the EP resin, suggesting that the difference in polarity of the organic monolayer and the epoxy resin led to partial deswelling of the clay. For the same reason, the exfoliated BzC16 layers collapsed in the presence of the epoxy resin, leading to the appearance of a reflection at 2.49° 2Θ. This confirms that the interplay of entropic and energetic factors governs the exfoliation and intercalation process.[36,37] Driving the solvent off and curing the epoxy resin led to almost complete deswelling of the sodium montmorillonite but did not affect the *d*-spacing of Bz1OH much, pointing out the incompatibility of EP with the inorganic silicate and the compatibility with Bz1OH. Increasing the Bz1OH filler concentration had no influence on the *d*-spacing, indicating that the intercalated polymer was not squeezed out on increasing the filler volume fraction. In the case of Bz2OH and Bz3OH, evaporating the solvent and curing the resin led to partial deswelling (0.28 nm), but there was an increase in *d*-spacing of the composites compared to the OM powder (0.12 and 0.46 nm, respectively), indicating polymer intercalation. Curing the BzC16, BzC18OH, and 2C18 composites led to further reduction in *d*-spacing, but it remained appreciable (2.9−3.5 nm). In comparison to the OM powder, there was an increase in *d*-spacing of 1.06, 1.39, and 0.95 nm, respectively, suggesting sizable intercalation. In contrast to Bz1OH, increasing the volume fraction of BzC16 from 0.01 to 0.05 led to gradual decrease in *d*-spacing from 3.07 to 2.90 nm, which suggests squeezing out of the intercalated polymer. This may support the notion that the epoxy resin reacts with the OH groups of BZ1OH. Unfortunately, no spectroscopic (IR) evidence could be obtained for this reaction. These results show that all OMs carrying long alkyl chains (BzC16, BzC18OH, 2C18) were strongly swollen by the solvent and intercalated by the polymer at the end, leading to an increase in *d*-spacing of 1 nm or more. The OMs with short alkyl chains (Bz1OH, Bz2OH, Bz3OH) were less swollen by the solvent and less intercalated by the epoxy polymer.

Since WAXRD does not give any information on the exfoliated part of the clay, the microstructure of the composites was investigated by TEM. Figure 2 shows TEM micrographs of the 3.5 vol % Bz1OH-EP composite. It can be seen that most of the OM particles were exfoliated to single layers (dark lines) or thin tactoids of very few layers that are flexible (bent) and misaligned. A similar observation has been made in PU nanocomposites.[7] It seems that it is not possible to align the montmorillonite platelets with the coating technique used. The composite of Bz2OH showed a similar morphology, but Bz3OH had more intercalated tactoids. The micrographs in Figure 3 represent the microstructure of the 3.5 vol % BzC16-EP composite, which consisted mainly of intercalated stacks. Some of these tactoids were thinner than the others, but all of them were misaligned and the *d*-spacing was ca. 3 nm in accordance with the WAXRD results. Figure 4 shows the microstructure of the 3.5 vol % composites of BzC18OH and 2C18, in which only very few single layers were observed. They practically consisted of intercalated tactoids, whose *d*-spacing corresponded to that measured by WAXRD (Table 2).

The oxygen permeability coefficients of the 3.5 vol % composites were measured (Table 3), and the relative permeability was plotted against the *d*-spacing in Figure 5. In contrast to all expectations, the relative permeability tendentially increased with increasing *d*-spacing, but no correlation between the two parameters could be found. This suggests that the intercalated part of the filler does not contribute much to the permeability

Table 2. Basal-Plane Spacing of the Fillers, Their Suspensions, and EP Composites

filler	*d*-spacing of filler powder [nm]	*d*-spacing of filler suspended in DMF [nm]	*d*-spacing of filler suspended in DMF + epoxy [nm]	*d*-spacing of EP composite [nm]
Cloisite Na^+ (3.5 vol %)	1.25	1.98	1.99	1.35
Bz1OH (1 vol %)	1.52			1.89
Bz1OH (2 vol %)				1.88
Bz1OH (3.5 vol %)		1.92	1.90	1.87
Bz1OH (5 vol %)				1.87
Bz2OH (3.5 vol %)	1.50	1.88	1.90	1.62
Bz3OH (3.5 vol %)	1.52	2.41	2.25	1.98
BzC18OH (3.5 vol %)	2.06	4.12	3.89	3.45
BzC16 (1 vol %)	1.87			3.07
BzC16 (2 vol %)				2.99
BzC16 (3.5 vol %)		no reflection	3.55	2.93
BzC16 (5 vol %)				2.90
2C18 (3.5 vol %)	2.51	3.69	3.54	3.46

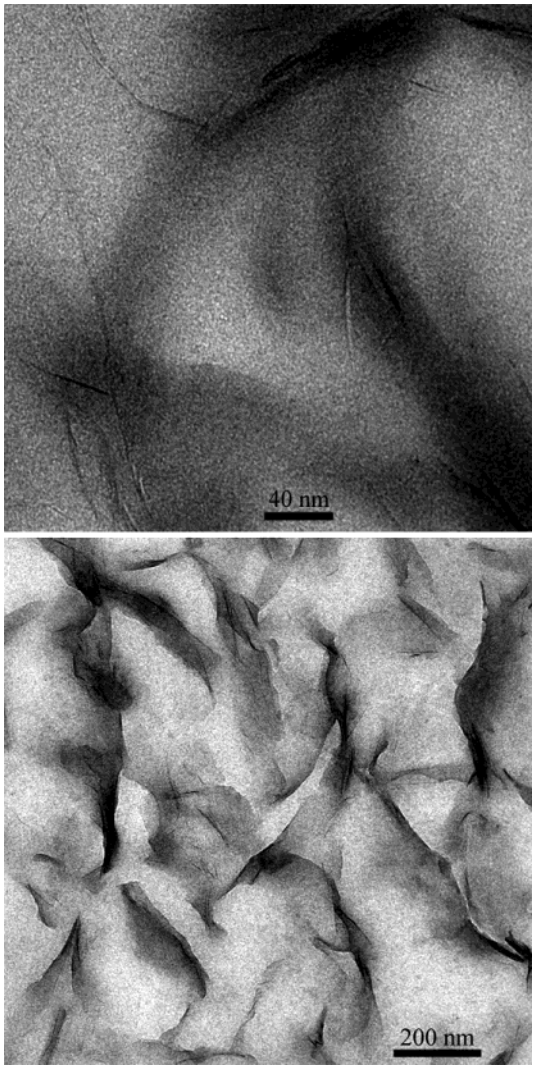

Figure 2. TEM micrographs of the 3.5 vol % Bz1OH−EP nanocomposite. The dark lines are cross sections of aluminosilicate layers or tactoids.

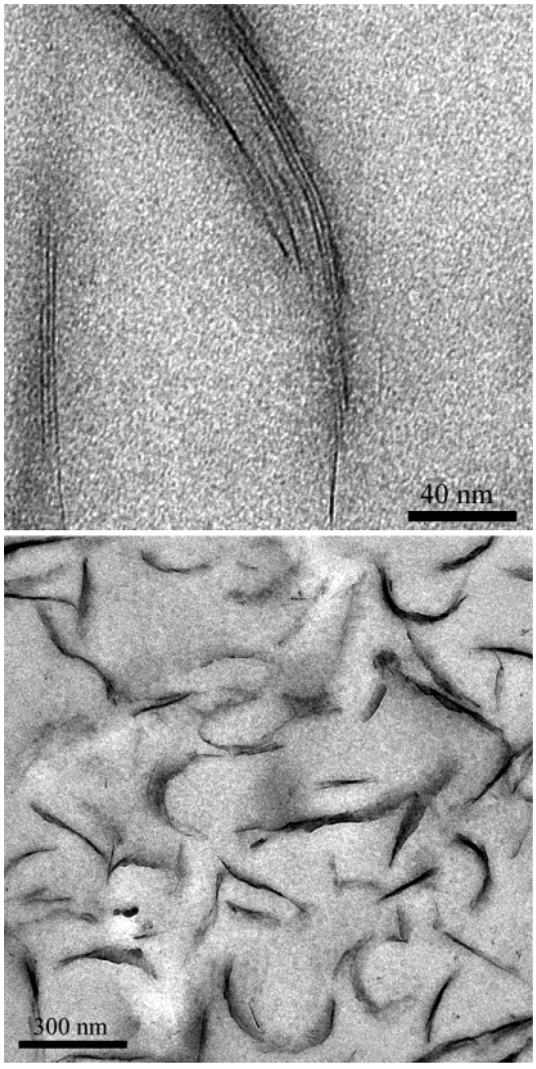

Figure 3. TEM micrographs of the 3.5 vol % BzC16−EP nanocomposite. The dark lines are cross sections of aluminosilicate layers or tactoids.

reduction and that the exfoliated layers are those which build the permeation barrier. This finding can be rationalized by realizing that the aspect ratio (longest axis/shortest axis) of the intercalated tactoids is not higher than that of the pristine OM, while that of the single layers can be as high as 300−400. It also confirms that the origin of the barrier performance of the inclusions in nanocomposites lies in the tortuous pathway the gas molecules have to go through. The permeability coefficient of the polymer matrix used is 60 times lower than that of the PP substrate but double that of the PET foils commonly used as an oxygen barrier. However, it is much lower than those of most adhesives commonly used in laminates, which do not contribute much to the barrier performance. The permeability coefficient of the BzC16 composite is the same as that of the sodium montmorillonite, which is 20% less than that of the neat polymer, while those of the BzC18OH and 2C18 composites are higher than that of the matrix. It seems that there is a phase separation between the long alkyl chains and the epoxy matrix, which leads to a decrease in density at the interface, resulting in higher "free volume" and consequently higher transmission rate. The same observation was made in 2C18−PU nanocomposites.[7] The presence of a hydroxyl group in BzC18OH did not help tethering polymer chains to the silicate surface. Probably, the long alkyl chain masks the OH group, hence hindering the reaction with the epoxy resin. Despite the low permeability of the polymer, Bz1OH and Bz2OH reduced the permeability coefficient two and half times, leading to a better oxygen barrier than PET. Bz3OH was less effective but still reduced the permeability coefficient of the polymer to half. These results are in accordance with the microstructure elicited by TEM and WAXRD, suggesting a reaction between the OH and epoxy groups or a good match between the surface energies of the two phases, leading to exfoliation of the OM to single layers. It seems that increasing the number of OH groups beyond a certain limit can be counterproductive due to increased polarity and hydrogen bonding. Interplay of entropic and energetic factors governs the exfoliation and intercalation process and is the key to designing the nanocomposite microstructure. The water vapor transmission rate through the polymer increased massively (230%) in the sodium montmorillonite composite but decreased by ca. 40% in the OM composites (Table 3). This reflects the difference in hydrophobicity of the fillers. The variety of chemical structure of the monolayer tested had little effect on the vapor transmission rate, and the values varied within a narrow range.

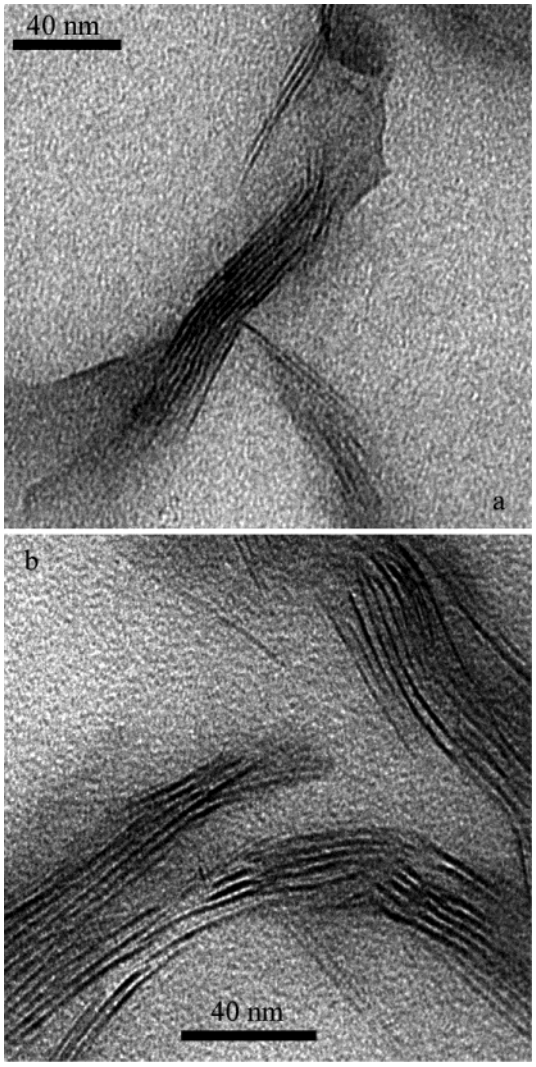

Figure 4. TEM micrographs of 3.5 vol % (a) BzC18OH−EP and (b) 2C18−EP nanocomposites. The dark lines are cross sections of aluminosilicate layers.

Table 3. Oxygen (0% RH) and Water Vapor Transmission Rates through 3.5 vol % OM−Epoxy Nanocomposites at 23 °C[a]

composite	permeability coefficient (oxygen) [$cm^3\ \mu m/(m^2\ d\ mmHg)$]	water vapor transmission rate [$g\ \mu m/(m^2\ d\ mmHg)$]
neat epoxy	2.0	10
Cloisite Na^+	1.6	23
Bz1OH	0.77	6.7
Bz2OH	0.78	5.8
Bz3OH	1.0	7.1
BzC18OH	2.2	5.7
BzC16	1.6	5.3
2C18	3.7	6.8

[a] Relative probable error 5%.

The effect of filler loading on the oxygen permeability coefficient and water vapor transmission rate of Bz1OH− and BzC16−EP nanocomposites, which represent a reactive and a nonreactive OM, respectively, is shown in Table 4. In both cases, the oxygen permeability coefficient decreased with increasing filler loading, but the reduction in the Bz1OH nanocomposites was more impressive, viz., factor of 4 at 5 vol % loading. The relative oxygen permeability is plotted in Figure 6 as a function of the inorganic volume fraction, showing that it decreases asymptotically with increasing filler loading. Theoretical models have shown that the relative permeability is a function of the inclusions aspect ratio, volume fraction, and orientation.[14−16] However, these models assume perfect parallel orientation, which is not the case here, and it is difficult to determine the aspect ratio of montmorillonite platelets in nanocomposites, especially in cases where mixed morphology is present and the silicate layers are bent or folded.[38] In such cases, a macroscopic average of the aspect ratio can better describe the geometry of the particles. Recently, the relative permeability of composites of misaligned disks has been numerically calculated as a function of the inclusions aspect ratio (diameter/thickness).[39,40] This

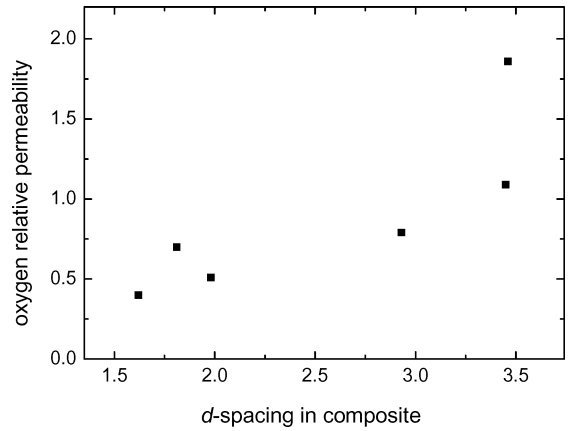

Figure 5. Oxygen relative permeability of the composites as a function of the *d*-spacing.

Table 4. Dependence of the Oxygen (0% RH) and Water Vapor Transmission Rates on Filler Loading at 23 °C[a]

composite	permeability coeff (oxygen) [$cm^3\ \mu m/(m^2\ d\ mmHg)$]	water vapor transmission rate [$g\ \mu m/(m^2\ d\ mmHg)$]
neat epoxy	2.0	10
Bz1OH (1 vol %)	1.4	8.9
Bz1OH (2 vol %)	0.91	8.0
Bz1OH (3.5 vol %)	0.77	6.7
Bz1OH (5 vol %)	0.55	5.7
BzC16 (1 vol %)	1.9	7.9
BzC16 (2 vol %)	1.7	6.5
BzC16 (3.5 vol %)	1.6	5.3
BzC16 (5 vol %)	1.6	4.9

[a] Relative probable error 5%.

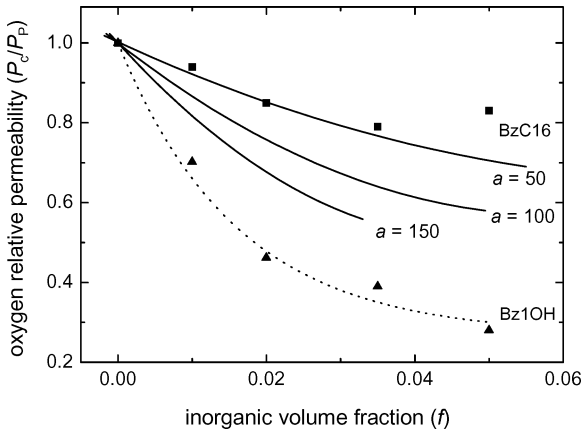

Figure 6. Oxygen relative permeability of Bz1OH− and BzC16−EP nanocomposites as a function of the inorganic volume fraction. The solid lines are numerical predictions for disk-shaped inclusions with aspect ratios 50, 100, and 150 (diameter/thickness), while the dotted line is simply a guide for the eye.

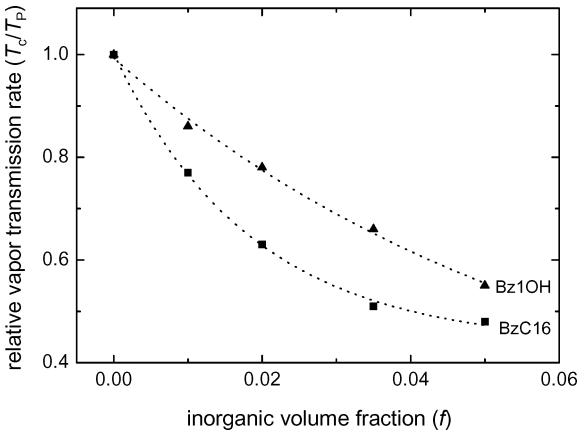

Figure 7. Water vapor relative transmission rate through Bz1OH− and BzC16−EP nanocomposites as a function of the inorganic volume fraction. The dotted line is simply a guide for the eye.

approach has been used here to estimate a macroscopic average of the aspect ratio of the inclusions as a function of filler loading. The solid lines in Figure 6 represent the numerical predictions for inclusions of aspect ratios 50, 100, and 150 at filler loading up to 5 vol %. For an aspect ratio of 150, it was not possible to obtain models of statistically misaligned disks with nonoverlapping configurations at loadings higher than 3 vol % as required by this approach. From Figure 6, it seems that the inclusions in the nonreactive OM composite (BzC16) have an aspect ratio of 50 but decreases at filler loadings higher than 3 vol %, probably due the dramatic decrease in interparticle distance and the consequent agglomeration above this concentration.[39,41] The reactive OM (Bz1OH) has much higher aspect ratio (250−300), corresponding to a very high degree of exfoliation in accordance with the TEM micrographs. It should be noted that the estimated aspect ratios are volume averages, which is usually higher than number averages. The relative transmission rate of water vapor through the BzC16 and Bz1OH composites is plotted in Figure 7 as a function of filler loading. The transmission rate decreases in both cases with increasing inorganic volume fraction, but the performance of BZC16 (factor of 2 at 5 vol %) is better than that of Bz1OH (40% at 5 vol %). This is in contrast to the oxygen permeability coefficient and reflects the hydrophobicity of the monolayer of the OMs, indicating that the permeant−composite interactions play an important role here. It is noteworthy to remark that all nanocomposites retained the optical properties of the polymer matrix.

Conclusions

Long alkyl chains increase the basal-plane spacing of organo-montmorillonites and enhance their swelling and intercalation. However, they do not lead to the desired improvement in composite properties unless the exfoliation is enhanced because the aspect ratio of the intercalated tactoids is not high. Alkyl chains seem to be incompatible with EP, which is aromatic to a large extent; therefore, they lead to an increase in *d*-spacing and in intercalation but not to exfoliation. Delaminated silicate layers have high aspect ratios and contribute most to the properties of nanocomposites. The exfoliation and intercalation process is governed by interplay of entropic and energetic factors, which is difficult to predict precisely. Tethering polymer molecules to the silicate layers enhances the exfoliation because these molecules cannot be squeezed out upon collapse of the layers. The aspect ratio of montmorillonite platelets is difficult to determine in polymer nanocomposites because of their flexibility which leads to bending and folding, aggravating the determination of their lateral dimension. Besides, a mixed morphology (exfoliated and intercalated structures) is often present, and the particle size of the inclusions is polydisperse, leading to a broad distribution of the aspect ratio. In such cases, a macroscopic volume average is well-suited to describe the anisometry of the particles. The aspect ratio can be deduced from the relative permeability of the nanocomposites to gas molecules by comparing the measured values to numerical predictions of the permeability in composites of misaligned disk-shaped inclusions. The incorporation of a small volume fraction of platelike nanoparticles in the epoxy matrix decreases its permeability coefficient to one-fourth. This can be attributed to the impermeability of the inorganic nanoparticles and the tortuous pathway the gas molecules have to cover during their random molecular motion in the composite. The transmission rate of water vapor through the composites is more influenced by the permeant−composite interactions and hence the hydrophobicity of the inclusions.

Acknowledgment. We gratefully acknowledge financial support from the Swiss National Science Foundation (SNF). We also thank NESTEC, Lausanne, and ALCAN PACKAGING, Neuhausen, for supporting the project.

References and Notes

(1) Bréchet, Y.; Cavaillé, J. Y.; Chabert, E.; Chazeau, L.; Dendievel, R.; Flandin, L.; Gauthier, C. *Adv. Eng. Mater.* **2001**, *3*, 571.
(2) Yano, K.; Usuki, A.; Okada, A.; Kurauchi, T.; Kamigito, O. *J. Polym. Sci., Part A: Polym. Chem.* **1993**, *31*, 2493.
(3) Giannelis, E. P. *Adv. Mater.* **1996**, *8*, 29.
(4) Gilman, J. W.; Kashiwagi, T.; Lichtenhan, J. D. *SAMPE J.* **1997**, *33*, 40.
(5) LeBaron, P. C.; Wang, Z.; Pinnavaia, T. J. *Appl. Clay Sci.* **1999**, *15*, 11.
(6) Alexandre, M.; Dubois, Ph. *Mater. Sci. Eng. R* **2000**, *28*, 1.
(7) Osman, M. A.; Mittal, V.; Morbidelli, M.; Suter, U. W. *Macromolecules* **2003**, *36*, 9851.
(8) Jasmund, K., Lagaly, G.; Eds. *Tonminerale und Tone;* Steinkopff-Verlag: Darmstadt, 1993.
(9) Osman, M. A.; Plötze, M.; Suter, U. W. *J. Mater. Chem.* **2003**, *13*, 2359.
(10) Lee, H.; Neville, K. *Handbook of Epoxy Resins*; McGraw-Hill: New York, 1967.
(11) Ellis, B. *Chemistry and Ttechnology of Epoxy Resins*; Blackie Academic & Professional: London, 1993.
(12) Sivis, H. C. *Trends Polym. Sci.* **1997**, *5*, 75.
(13) Brennan, D. J.; Haag, A. P.; White, J. E.; Brown, C. N. *Macromolecules* **1998**, *31*, 2622.
(14) Eitzman, D. M.; Melkote, R. R.; Cussler, E. L. *AIChE J.* **1996**, *42*, 2.
(15) Fredrickson, G. H.; Bicerano, J. *J. Chem. Phys.* **1999**, *110*, 2181.
(16) Gusev, A. A.; Lusti, H. R. *Adv. Mater.* **2001**, *13*, 1641.
(17) Messersmith, P. B.; Giannelis, E. P. *Chem. Mater.* **1994**, *6*, 1719.
(18) Lan, T.; Kaviratna, P. D.; Pinnavaia, T. J. *Chem. Mater.* **1995**, *7*, 2144.
(19) Zilg, C.; Mülhaupt, R.; Finter, J. *Macromol. Chem. Phys.* **1999**, *200*, 661.
(20) Brown, J. M.; Curliss, D.; Vaia, R. A. *Chem. Mater.* **2000**, *12*, 3376.
(21) Zerda, A. S.; Lesser, A. J. *J. Polym. Sci., Part B: Polym. Phys.* **2001**, *39*, 1137.

(22) Kornmann, X.; Lindberg, H.; Berglund, L. A. *Polymer* **2001**, *42*, 1303.
(23) Kornmann, X.; Thomann, R.; Mülhaupt, R.; Finter, J.; Berglund, L. *J. Appl. Polym. Sci.* **2002**, *86*, 2643.
(24) Kong, D.; Park, C. E. *Chem. Mater.* 2003;*15*, 419.
(25) Vaia, R. A.; Liu, W. *J. Polym. Sci., Part B* **2002**, *40*, 1590.
(26) Morgan, A. B.; Gilman, J. W. *J. Appl. Polym. Sci.* **2003**, *87*, 1329.
(27) Shimauchi, S.; Minemura, I.; Matsui, K.; Shirasawa, K. *Jpn. Tokkyo Koho* **1973**, JP 48006664; CAN 80:49134.
(28) Smirnova, A. T.; Kabanov, V. P.; Kharkov, S. N.; Ivanova, L. A. *J. Appl. Chem. USSR* **1987**, *60*, 534.
(29) Hayashi, Y.; Fujiwara, T.; Shimizu, T.; Nagano, Y.; Teramura, K. *Yukagaku* **1987**, *36*, 409; CAN 108:74771.
(30) Al-Sabbagh, A. M.; Osman, M. M.; Omar, A. M. A.; El-Gamal, I. M. *Anti-Corros. Method Mater.* **1996**, *43*, 11.
(31) Li, Z.; Fu, L.; Chen, Z. *Huagong Daxue Xuebao* **1999**, *26*, 61, CAN 132:266475.
(32) Osman, M. A.; Suter, U. W. *J. Colloid Interface Sci.* **2000**, *224*, 112.
(33) Osman, M. A.; Plötze, M.; Skrabal, P. *J. Phys. Chem. B* **2004**, *108*, 2580.
(34) Balazs, A. C.; Singh, C.; Zhulina, E.; Lyatskaya, Y. *Acc. Chem. Res.* **1999**, *32*, 651.
(35) Ginzburg, V. V.; Singh, C.; Balazs, A. C. *Macromolecules* **2000**, *33*, 1089.
(36) Vaia, R. A.; Giannelis, P. *Macromolecules* **1997**, *30*, 7990.
(37) Vaia, R. A.; Giannelis, P. *Macromolecules* **1997**, *30*, 8000.
(38) Fornes, T. D.; Paul, D. R. *Polymer* **2003**, *44*, 4993.
(39) Osman, M. A.; Mittal, V.; Lusti, H. R. *Macromol. Rapid Commun.* **2004**, *25*, 1145.
(40) Lusti, H. R.; Gusev, A. A.; Guseva, O. *Adv. Mater.*, submitted.
(41) Vaia, R. A. In *Polymer-Clay Nanocomposites*; Wiley: Chichester, 2000; p 229.

MA048798K